PHYSICAL REVIEW E **85**, 056403 (2012)

Time-dependent ionization models designed for intense and short laser pulse propagation in dielectric materials

Antoine Bourgeade[1,*] and Guillaume Duchateau[2,*]
[1]*CEA/CESTA, BP2, 33114 Le Barp, France*
[2]*CELIA, UMR 5107 Université Bordeaux 1-CNRS-CEA, 33405 Talence Cedex, France*

(Received 22 December 2011; published 15 May 2012)

When an intense and short laser pulse propagates in a dielectric material, significant production of conduction electrons through multiphoton absorption (MPA) may occur. In addition to the laser intensity, the MPA process depends mainly on the laser frequency spectrum which may evolve significantly during the course of laser propagation in the material. Simple models for MPA accounting for possible time-dependent evolution of the laser frequency spectrum (as harmonic generation, chirping or broadening) are addressed. The first model is based on Bloch-Volkov states whereas the second approach relies on the density matrix formalism which has been adapted for the present study. Both models are well adapted for their introduction in a propagation code and are shown to correctly account for the MPA process whatever the characteristics of the laser frequency spectrum. The reliability of these approaches has been studied in two cases of practical interest. First, in the case where a second harmonic is present within the fundamental pulse, calculations show that the ionization rate may be significantly enhanced. Second, in the case of a chirped pulse, models are shown to correctly account for possible change in the multiphoton order during the course of interaction.

DOI: 10.1103/PhysRevE.85.056403 PACS number(s): 52.50.Jm, 52.25.Tx, 79.20.Ws

I. INTRODUCTION

Dielectric materials with a large band gap (such as silica, LBO, BBO, KDP, KTP, sapphire, etc.) are widely used in current lasers as optical materials, allowing one to transform the pulse characteristics. In the case of short (femtosecond) and intense laser pulses, material and pulse shape may be strongly perturbed due to the following processes: promotion of valence electrons to the conduction band through multiphoton absorption (MPA), laser heating of conduction electrons, and possibly electron avalanche through impact ionization [1,2]. These interactions may lead to the formation of a plasma state at a density close to the solid one, i.e., the so-called warm dense matter (WDM). For high intensities, this strong laser-matter coupling can lead to a significant modification of the time-evolution laser intensity and damage of the optical material may take place [1,3,4]. Material modifications following laser-matter interaction may be desired to achieve the so-called nano-structuration of materials whose applications can be light-guiding devices or grating manufacturing [5]. Whether to prevent undesired material modifications or to control nano-structuration, there is a need to accurately describe the above-mentioned physical phenomena and correctly model the laser pulse propagation. In particular, since the interaction is initiated by the ionization stage, a time-dependent description of this process is required [6–8].

Modeling the laser pulse propagation is achieved by solving the Maxwell's equations [9–11] where the interaction with matter is included through the energy transfer from the laser beam to the dielectric material. Multiphoton ionization (MPI, i.e., transition from the valence band to the conduction band through the simultaneous absorption of several photons) and subsequent heating via inverse Bremstrahlung thus should be modeled. Many theories have been developed to evaluate the ionization rate of atoms or solids by strong laser fields, which are essentially based on the electric dipole approximation. The pioneering work of Keldysh [12,13] showed that multiphoton ionization and tunnel ionization are two limit cases of a more general phenomenon of nonlinear photoionization. He defined the now largely used Keldysh parameter which governs this process. Later, Perelomov, Popov, and Terent'ev [14,15] adapted this theory to more complex ions (PPT theory), and Ammosov, Delone, and Krainov (ADK) included the effect of the ion Coulomb field [16].

Those theories are adapted to describe the MPI process induced by a monochromatic pulse propagating in amorphous dielectric materials (such as fused silica or sapphire, for instance) which are known not to modify the frequency spectrum. Indeed, the formula for MPI is based on the Keldysh parameter which includes the laser frequency that should be explicitly known. In the case of pulse propagation through dielectric materials aiming at reshaping the frequency spectrum, the above-mentioned models cannot be used since a single laser frequency cannot be defined explicitly. For instance, with an optical parametric chirped-pulse amplification (OPCPA) system and KDP crystals, the frequency spectrum may be spread or frequency conversion may occur during the course of propagation. It follows that the multiphoton order may evolve with time [6]. The way to accurately evaluate the MPI induced by a laser pulse exhibiting a relatively large time-dependent frequency spectrum is to derive a model based on the knowledge of the laser electric field which implicitly contains all information regarding the time-dependent frequency spectrum. This space and time-dependent electric field can be provided by a numerical code solving the 3D Maxwell's equations (hereafter called CME). It is worth noting that CME consumes large amounts of CPU time and, thus, requires a simple model to describe the above-mentioned laser interaction with matter.

The approaches based on numerical resolution of the time-dependent Schrödinger equation (TDSE) are generally

---

[*] antoine.bourgeade@cea.fr; duchateau@celia.u-bordeaux1.fr

cumbersome and are not suitable within the present framework to describe MPI. Recent papers [17–19] have considered models of atom ionization by ultrashort laser pulses based on the knowledge of the laser electric field. They dealt with the electron energy distribution and considered very strong laser pulses. These methods are complex and, thus, not well adapted for their introduction in a CME. In order to describe the MPI in a consistent and tractable way in codes aiming to describe pulse propagation in dielectric materials, there is a need to develop a simple model which accounts for the evolution of the frequency spectrum with respect to time.

The present paper addresses the development of such simple MPI models for dielectric materials, which are based on the knowledge of the time-dependent laser electric field. They are designed for future studies of pulse propagation which may not be carried out currently with the state-of-the-art methods. It is noteworthy that those simple models also represent an alternative to current theoretical developments dealing with MPI, even without invoking pulse propagation considerations. Hereafter are proposed two approaches, based on different assumptions, both relying on the electric dipole approximation and a single-active electron within the length gauge. Furthermore, linearly polarized laser pulses are considered in the present study. The first approach, called BVkP, is based on an evaluation of the transition amplitude with Bloch-Volkov (BV) wave functions [20] used to describe the multiphoton absorption. Under this framework, the evaluation of matrix elements can be performed by utilizing the $\vec{k}\cdot\hat{P}$ theory [21,22] which provides accurate results in the center of the Brillouin zone (BZ). The second approach, called the optical Bloch (OB) method, is based on the resolution of the Liouville equation governing the evolution of the density matrix [23–25]. It has been adapted to the present case of interest, leading to a tractable and efficient MPI model. The BVkP approach is relevant for perturbative conditions, whereas the OB model should be able to make accurate predictions for very high intensities with a possible significant depletion of the valence band. However, the OB model depends, more than the BVkP, on free physical parameters (related to the electronic structure). It follows that, depending on the laser pulse characteristics and on the knowledge of the electronic structure of the material, one or another method could be more adapted to efficiently describe the time-dependent MPI process. In addition to the possibility of considering a larger range of physical conditions of interest, the development of two models allows us to check the reliability of our approach. Indeed, since both models are developed within the same framework, the same trends for predictions are expected. As will be shown, the previous approaches account for the fact that an ionized electron can go back to the valence band through the action of the electromagnetic field. However, this coherence may be broken in a condensed matter where the excited electrons may undergo collisions with phonons, ions, or other electrons. This phenomenon may significantly affect the evolution of the free electron density which is used in the CME to derive the electron current. It has been taken into consideration through an *ad hoc* method based on a relaxation process. The previous theoretical developments are the subject of Sec. II. Since we are mainly interested in the derivation of a photon-ionization rate responsible for the initiation of significant laser-matter coupling, the impact ionization mechanism is not considered in the present work.

In Sec. III the proposed models have been numerically developed and applied to various physical cases. First, in the monochromatic case, the reliability of the proposed approaches is checked: The ionization rates are studied as a function of time, photon energy, and laser intensity. For each study, both modeling predictions are compared and discussed. In particular, this study demonstrates that both the BVkP and OB models are able to account for multiphoton absorption. In order to check the reliability of the proposed approaches in conditions relevant for frequency conversion, a case where the electric field contains two different frequencies is considered. In this situation, each model accounts for two different multiphoton orders, thus demonstrating that the multiphoton order may evolve in time. Finally, the present approaches are applied in conditions of major interest where MPI is induced by a chirped pulse, i.e., for a laser frequency depending on time. In that case, both models are shown to account for possible change in the multiphoton order during the course of interaction.

Conclusions are addressed in Sec. IV. Atomic units are used throughout the modeling Sec. II unless otherwise stated.

II. MODELING

A. The BVkP model

This section is devoted to the establishment of an ionization model based on an approximated evaluation of the electron wave function in both the crystal potential and the electric field of the laser pulse. From a general point of view, within the electric dipole approximation, the transition amplitude from the initial valence band to the final conduction band is given by

$$T_{cv}(t) = -i\int_0^t dt\,\langle\Psi_c(t)|\vec{r}\cdot\vec{E}(t)|\varphi_v(t)\rangle, \tag{1}$$

where $\Psi_c(t)$ is the perturbed one-electron wave function related to the conduction band and $\varphi_v(t)$ is the nonperturbed valence wave function. These states are solutions of the following Schrödinger equations:

$$H\Psi_c(t) = i\frac{\partial\Psi_c(t)}{\partial t} \tag{2}$$

and

$$H_0\varphi_v(t) = E_v\varphi_v(t), \tag{3}$$

where

$$H = H_0 + H_{\text{int}} \quad \text{with} \quad H_0 = -\frac{\nabla^2}{2m} + V(\vec{r}) \quad \text{and} \quad H_{\text{int}} = \vec{r}\cdot\vec{E}(t), \tag{4}$$

$V(\vec{r})$ being the crystalline potential and $\vec{E}(t)$ the laser electric field. It can be shown that a reliable approximation of $\Psi_c(t)$ is given by a Bloch-Volkov wave function [20] that reads,

$$\Psi_c(t) \simeq \chi_c^{\text{BV}}(t) = \varphi_c(t)\exp\left\{i\vec{A}(t)\cdot\vec{r} - i\int_0^t dt'\frac{[A(t')]^2}{2m}\right\}, \tag{5}$$

where $\vec{A}(t)$ is the vector potential given by $\vec{A}(t) = -\int_0^t dt'\vec{E}(t')$. The Volkov phase accounts for the dressing of electrons by photons [26] and renders it possible to account for the simultaneous absorption of several photons. This approach has been successfully used to model the multiphoton ionization of atoms [26–31]. However, within this framework, it was shown that the phase $\exp(i\int_0^t dt' A^2(t')/2)$ introduces spurious behaviors [30]. Further, contrary to the term $\exp(i\vec{A}\cdot\vec{r})$, it is noteworthy that that the phase $\exp[i\int_0^t dt' A^2(t')/2]$ does not induce any transition [32]; it only slightly shifts the energy spectrum in cases of long or intense laser pulse where the ponderomotive energy is significant. Therefore, this term is hereafter omitted.

There is no simple and realistic expression for the unperturbed wave functions $\varphi_v(t)$ and $\varphi_c(t)$. It follows that the matrix element $\langle\chi_c^{\mathrm{BV}}(t)|\vec{r}\cdot\vec{E}(t)|\varphi_v(t)\rangle$ cannot be simply evaluated at first glance. The cornerstone of the present approach is to introduce matrix elements which can be evaluated within the $\vec{k}\cdot\vec{P}$ theory [21,22]. To do so, the Volkov phase is developed in series as

$$\exp\{i\vec{A}(t)\cdot\vec{r}\} = \sum_{n=0}^{\infty}\frac{[i\vec{A}(t)\cdot\vec{r}]^n}{n!}. \tag{6}$$

This development makes sense for a small vector potential amplitude, i.e., within a framework relevant for perturbative conditions. The transition amplitude (1) thus reads,

$$T_{cv}(t) = -i\int_0^t dt\exp\{i(E_c - E_v)t\} \times \sum_{n=0}^{\infty}\frac{1}{n!}\langle\phi_c|(i\vec{A}(t)\cdot\vec{r})^n(\vec{r}\cdot\vec{E}(t))|\phi_v\rangle, \tag{7}$$

where $\varphi_j(\vec{r},t) = \phi_j(\vec{r})\exp(-iE_jt)$ with $j = v$ or c. Now, we have to evaluate the matrix element

$$M_n(t) = \langle\phi_c|(i\vec{A}(t)\cdot\vec{r})^n(\vec{r}\cdot\vec{E}(t))|\phi_v\rangle. \tag{8}$$

Since it implies a dipolelike term to the power $n+1$, this matrix element accounts for the absorption of $n+1$ photons. In particular, the case $n = 0$ (M_0, absorption of only one photon) corresponds to the standard first-order pertubation theory (Born approximation) where the wave functions corresponds to nonperturbed states. The $\vec{k}\cdot\hat{P}$ theory allows one to establish the following relation [21,22]:

$$P = \langle\phi_c|\hat{P}_Z|\phi_v\rangle = \sqrt{\frac{m_0^2E_g}{2m_{vc}^*}} \quad \text{with} \quad \frac{1}{m_{vc}^*} = \frac{1}{m_v^*} + \frac{1}{m_c^*}, \tag{9}$$

where $\vec{P} = -i\vec{\nabla}$ is the momentum operator. Note that under the $\vec{k}\cdot\hat{P}$ framework, expression (9) is valid only in the center of the Brillouin zone (BZ), which makes sense in the present study since we are dealing with direct gap dielectrics. Due to the properties of the position and momentum operator [33], it turns out that

$$M_0(t) = \frac{E(t)P}{im_0(E_c - E_v)}. \tag{10}$$

Furthermore, the matrix element M_n can be expressed as a function of M_0. In order to establish this relation, we approximate the wave functions by simple expressions but which include the major physical trends (see Appendix A). Under these approximations, the following relation stands:

$$M_n(t) = \frac{[iA(t)]^n(-1)^n(n+1)!}{(-\alpha + ik)^n}M_0(t), \tag{11}$$

where k is the electron momentum of free states and α is related to the valence state, accounting for the spatial localization of this bound wave function. The transition amplitude thus reads,

$$T_{cv}(t) = -i\int_0^t dt\exp\{i(E_c - E_v)t\} \times \sum_{n=0}^{\infty}\frac{1}{n!}\frac{[iA(t)]^n(-1)^n(n+1)!}{(-\alpha + ik)^n}\frac{E(t)P}{im_0(E_c - E_v)}. \tag{12}$$

Since transitions mainly occur in the center of the BZ in direct gap dielectrics, it follows that setting $k = 0$ in Eq. (12) is a reliable approximation. One thus obtains,

$$T_{cv}(t) = -\frac{P}{m_0(E_c - E_v)}\int_0^t dt\exp\{i(E_c - E_v)t\}E(t) \times \sum_{n=0}^{\infty}(n+1)i^n\left[\frac{A(t)}{\alpha}\right]^n. \tag{13}$$

In the case where $x = |A(t)/\alpha|$ verifies $x < 1$ for any time during the interaction, the following relation stands:

$$\sum_{n=0}^{\infty}(n+1)(ix)^n = \frac{1}{(1 - ix)^2}. \tag{14}$$

Note that in the case of intense or long pulses, the previous relation no longer stands. This situation corresponds to nonperturbative conditions where transition amplitudes with various multiphoton orders may become comparable [34]. Finally, within this approach, the transition amplitude from the VB to the CB reads,

$$T_{cv}(t) = -\frac{P}{m_0(E_c - E_v)}\int_0^t dt\exp\{i(E_c - E_v)t\} \times \frac{E(t)}{(1 - iA(t)/\alpha)^2}. \tag{15}$$

The ionization rate W_{MPI}, i.e., the number of valence electrons promoted in the conduction band per unit of time and volume, is then given by

$$W_{\mathrm{MPI}}(t) = N_0\frac{\partial|T_{cv}(t)|^2}{\partial t} = 2N_0\,\mathrm{Re}\left\{T_{cv}^*(t)\frac{\partial T_{cv}(t)}{\partial t}\right\}, \tag{16}$$

where N_0 is the density of valence electrons, set to $2.2 \times 10^{22}\ \mathrm{cm}^{-3}$ in the present study. From a general point of view, numerous conduction states may exist in dielectric material [35]. Depending on the photon energy, a valence electron then can be promoted to different energy levels corresponding to different conduction states. In order to account for this fact, various final states, called c_i, should be taken into consideration. The according ionization rate is obtained by substituting $\sum_i|T_{c_iv}(t)|^2$ for $|T_{cv}(t)|^2$ in Eq. (16). This is done numerically in a way to avoid the ionization rate being greater than 1 and to have an ionization rate depending as little as possible from the number of states describing a conduction band.

B. The optical Bloch model

Another way to model the ionization process is the optical Bloch (OB) model. The basis of this approach is presented in Refs. [24,25] along with its adaptation to the MPI description, allowing one numerical calculations as fast as possible, is provided. This method is adapted to any number of levels and is easy to associate with Maxwell equations to model the propagation of a laser pulse [36,37]. As in the previous model, we consider the wave function of a valence or conduction electron under the action of the electromagnetic field. It is the solution of a Schrödinger equation (2) where the Hamiltonian is the sum of the unperturbed Hamiltonian, H_0, and of the interaction Hamiltonian (4), H_{int}. For this interaction Hamiltonian, only the electric dipole momentum is considered. However, instead of looking for the transition amplitude, the OB model aims at describing the time evolution of the density matrix which, for a state vector $|\psi\rangle$, is defined by

$$\rho = |\psi\rangle\langle\psi|. \tag{17}$$

If $|\psi\rangle$ is given by its projection on N eigenstates of the unperturbed Hamiltonian, ρ is an $N \times N$ semidefinite positive and Hermitian matrix. In each point of the computational domain there is more than one atom to consider. Therefore, the density matrix is associated to an ensemble of atoms around this point. It is defined by

$$\rho = \sum_S p_S |\psi_S\rangle\langle\psi_S|, \tag{18}$$

where S belongs to a statistical ensemble of states and p_S is the probability for these states to be characterized by the state vector $|\psi_S\rangle$. The temporal evolution of ρ is governed by the Liouville-von Neumann equation [23],

$$i\frac{\partial}{\partial t}\rho(t) = [H,\rho] = H\rho - \rho H. \tag{19}$$

The diagonal elements of ρ provide the occupation rates of the various levels, while the extradiagonal elements describe the coherence between levels. The sum of the diagonal elements associated to the conduction band then provides the density of conduction electrons. Its time derivative thus renders it possible to evaluate the instantaneous ionization rate. The Liouville-von Neumann equation can be rewritten as

$$i\frac{\partial}{\partial t}\rho_{jk}(t) = (E_j - E_k) + \mathbf{E}(t)\cdot\sum_{l=1}^{N}\rho_{jl}(t)\boldsymbol{\mu}_{lk} - \mathbf{E}(t) \cdot \sum_{l=1}^{N}\rho_{lk}(t)\boldsymbol{\mu}_{jl}, \tag{20}$$

where E_j is the energy associated to the level j and $\boldsymbol{\mu}_{jl} = \langle\psi_j|\vec{r}|\psi_l\rangle$ is the matrix element of the operator $\vec{r}$ which accounts for the coupling of state ψ_j to state ψ_l due to the action of the laser electric field. In the present approach, it is assumed that $\mu_{ii} = 0$, i.e., wave functions are assumed to have a well-defined parity [38]. Since we are interested only in the ionization rate, we may consider, first, the level in the valence band and the other in the conduction band with connections ($\mu_{jl} \neq 0$) only between the valence state and the ionization states. Within this configuration, the OB approach cannot account for MPI with an even number of absorbed photons (see Appendix B). To avoid this drawback, we have introduced two states in the valence band. These two states are connected together and connected with all the states in the conduction band. With this configuration we are able to describe photoionization with any number of photons as soon as the laser intensity is high enough. Moreover, this model is able to take into account as many states in the conduction band as necessary. The choice of the nonzero elements μ_{jl} provides many degrees of freedom for the model. In order to get an ionization rate as independent as possible on the number N_C of states in the conduction band, we chose those elements to be equal and inversely proportional to $\sqrt{N_C}$. Doing so introduces a normalization. Only the element connecting the two states in the valence band can differ.

In practice, the time evolution of the density matrix is obtained with the following relation deduced from Eq. (20):

$$\rho(t+\delta t) = \exp\left[i\int_t^{t+\delta t} H(\tau)d\tau\right]\rho(t) \times \exp\left[-i\int_t^{t+\delta t} H(\tau)d\tau\right]. \tag{21}$$

In the numerical resolution, this solution is approached for the time step between t and $t + \delta t$ by the following expression:

$$\rho(t+\delta t) = \left[\mathrm{Id} + \frac{i}{2}H\left(t+\frac{\delta t}{2}\right)\right]\left[\mathrm{Id} - \frac{i}{2}H\left(t+\frac{\delta t}{2}\right)\right]^{-1} \times \rho(t)\left[\mathrm{Id} - \frac{i}{2}H\left(t+\frac{\delta t}{2}\right)\right] \times \left[\mathrm{Id} + \frac{i}{2}H\left(t+\frac{\delta t}{2}\right)\right]^{-1}, \tag{22}$$

where Id is the identity matrix. This approximation avoids the computation of the exponential matrix and guarantees at any time the right properties for the density matrix $\rho(t)$: Its trace is always equal to 1 and it is a positive semidefinite Hermitian matrix. Moreover, this numerical scheme is of the order 2 in time. We can also notice that, thanks to the choice we have made for the nonzero element of the matrix μ, the inversion of the matrix $[\mathrm{Id} + \frac{i}{2}H(t+\frac{\delta t}{2})]$ can be done analytically: It is equivalent to solving a 2×2 system whatever the value of N_C (see Appendix C). This scheme is, thus, relatively easy to implement.

C. Introduction of a relaxation state for laser heating of conduction electrons

Within the framework of the previous approaches, an excited electron can interact only with the laser electric field and its parent ion. However, in condensed matter, excited electrons generally undergo collisions with other particles such as phonons, ions (other than the parent), or other electrons making the plasma. Those collisions render it possible for a conduction electron to be heated by the laser pulse, as described, for instance, by the Drude model. When such a collision occurs, the coherence between the excited electron and its parent ion vanishes. We can define a free state as an electronic state whose associated electrons can be heated by inverse Bremstrahlung and which is decorrelated from the parent ion. We call the free electron density the density of electrons associated with this free state. In the CME, this free electron density is the one required to evaluate the electron current [10,11]. Furthermore, in order to model impact ionization, an approach as proposed by Rethfeld [2] may be implemented in the CME. Within this framework, the present free state may act as a starter to transitions toward states with higher energies.

As it will be shown in the next section, since collisions are not included in the modeling, the present models for ionization are reversible in the sense where they predict significant variations of the density of conduction electrons with respect to time, accounting for the fact that a conduction electron may go back to the valence band through the action of the electromagnetic field. This process is particularly important when we are far from resonance (photon energy close to energy difference between the bridged states). In order to introduce irreversibility, accounting for collisions and decoherence, and leading to an ionization rate consistent with the CME and condensed matter properties, we had the choice between two solutions. We could suppress the hypothesis of no electromagnetic connection between the states in the conduction band and introduce relaxation processes between all the states. The other solution would be to introduce a new state in the conduction band on which all the other states from this band can relax but is not connected to any other state (all the corresponding elements of the μ matrix are zeros). This state represents the free electrons which will be accelerated by the electromagnetic field and thus can no longer recombine reversibly and coherently with the parent ions. We have retained the second solution because it is the only one we could use for both models and because, in this approach, we are interested only in the ionization rate.

Thus, this new relaxation state is simply added in the Bloch model where the density matrix is modified at each time step in order to take the action of the relaxation terms into account. For the BVkP model, we compute at each time step, and for each initial state in the conduction band, the number of electrons which relax on the new state and add these contributions to the previous number of electrons in this relaxation state.

The value of the relaxation time may be on the order of the picosecond timescale. Indeed, femtosecond time-resolved interferometry experiments have shown that conduction electrons may relax in KDP crystals on a timescale ranging from roughly 300 fs to tens of ps [39]. Further, the same order of magnitude for other wide-band-gap dielectric materials, such as NaCl, MgO, or Al_2O_3, was measured [40–42]. We thus use 3 ps according to these relaxation time measurements. This value is used throughout the paper unless otherwise stated. It is worth noting that slight deviations from this value do not change the results presented in Sec. III significantly. Also, note that the value of the relaxation time should be adapted depending on the material of interest.

Since the rate for the valence-conduction transition is known with the BVkP approach, the evaluation of the electron population associated with the free state is simply obtained by solving the standard rate equation where the characteristic relaxation time τ_r is included. Regarding the OB model, the evaluation of the free electron density is simply obtained by adding the state of interest. However, note that the latter state is not coupled through the electromagnetic field to the other ones. Furthermore, for both approaches, the depletion of the initial valence state is introduced.

III. RESULTS AND DISCUSSION

A. Ionization induced by one laser pulse

As a preliminary remark, simple estimates of impact ionization contribution to the final density of conduction electron can be obtained from the results of Rethfeld [2]. Within our conditions (laser pulse duration of 100 fs and intensity lower than 5×10^{13} W/cm^2), Fig. 6 of Ref. [2] shows that percentiles of the fraction of impact-ionized electrons is less than 5%, thus negligible compared to multiphoton ionization. It follows that the proposed models for ionization are sufficient to correctly predict the ionization. Impact ionization should be included in CME for intensities in excess of 10^{14} W/cm^2.

Before considering the evolution of the free electron density with respect to the laser pulse parameters, let us study the temporal evolution of the ionization rate predicted by the BVkP and the OB approaches. In order to compare both models, their free parameters have been set as follows. Regarding the BVkP approach, the parameter α has been set to 1.55 a.u. This value allows one to reproduce correctly the predictions of the Keldysh formula [12] for laser parameters of interest for this work. Note that this value of α is consistent with the common spatial extension of a bound state. Moreover, slight variations of this value do not change the conclusions of the present study. The parameters of the OB model have been set in order to mimic the BVkP ionization rate during the early stage of the process. Also, $\mu_{vv} = 1.68 \times 10^{-29}$ Cm and $\mu_{vc} = 1.34 \times 10^{-29}$ Cm have been used, whatever the energy of the conduction state. It is noteworthy that those values of the modeling parameters are used throughout the present paper. Under these conditions, Fig. 1 shows the temporal evolution of the laser-induced electronic density as directly predicted by both models (no relaxation into the free state occurs here). For this calculation, the laser pulse characteristics are as follows: $I = 5 \times 10^{13}$ W/cm^2, $\tau = 100$ fs, $\lambda = 413$ nm (close to the second harmonic of the Ti:sapphire laser), and a temporal sine envelope has been used as $E(t) = E_0 \sin(\omega t) \sin(\pi t/\tau)$. With the latter wavelength, three photons are required to bridge the band gap (set to 9 eV). As expected, both models exhibit the same trends. Further, it appears that the electronic density oscillates as a function of time, accounting for the fact that the electron oscillates back and forth around the parent ion due to the driving laser electric field. Indeed, we have checked that the observed frequency is the same as the laser one. During this process, however, it turns out that the electron can be ionized and recombine leading to a nonzero ionization probability at the end of the pulse.

As discussed in Sec. II C, since we are dealing with a condensed matter, during the interaction, an ionized electron may undergo a collision on a particle present in the vicinity of the

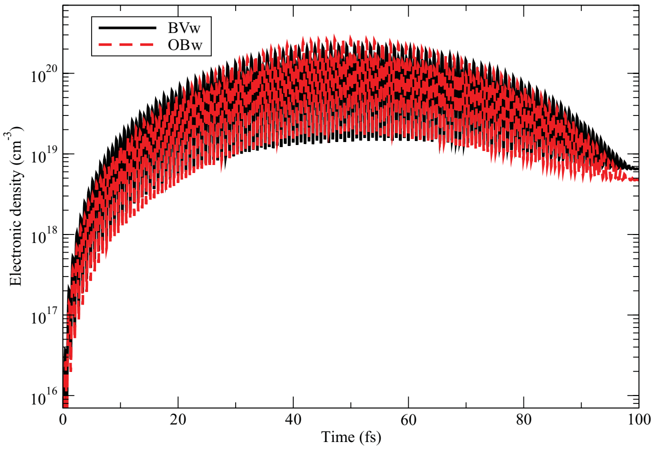

FIG. 1. (Color online) Evolution of the electronic density in the conduction band as a function of time, as directly predicted from the ionization rate. The black (solid) and the red (dashed) curves correspond to predictions of the BVkP and OB model, respectively. For both models, calculations have been performed with 81 energy levels. The laser pulse parameters are as follows: $I_0 = 5 \times 10^{13}$ W/cm^2, $\tau = 100$ fs, and $\lambda = 413$ nm. The latter parameter corresponds to the situation where three photons are required to bridge the band gap.

parent ion as another ion, electron, or phonon. In that case, the coherence between the initial valence state and the conduction state is broken, leading to an irreversible detachment of the electron from the parent ion and subsequently producing free electrons. With the same parameters as those of Fig. 1, the evolution of the free electron density is shown in Fig. 2. As for the ionization rates, both models predict the same trend, i.e., a free electron density increasing monotonically with respect to time. In order to evaluate the influence of the value of the relaxation time, additional calculations with a relaxation time of 1 and 5 ps have been performed. As expected, these results show that the longer the relaxation time, the smaller the electronic density associated with the free state. Note that the final density, close to 2×10^{18} cm^{-3} for this study or close to 10^{20} cm^{-3} for a two-photon absorption (see Fig. 4), corresponds to orders of magnitude commonly observed under such conditions for various dielectric materials [39–42]. Electronic density on the order of 10^{20} cm^{-3} in α-quartz, induced by two-photon absorption with laser pulse parameters comparable to those presently used (see Fig. 4), have also been predicted by use of first-principles calculations [43,44]. These comparisons thus provide a confirmation of the validity of the proposed approaches.

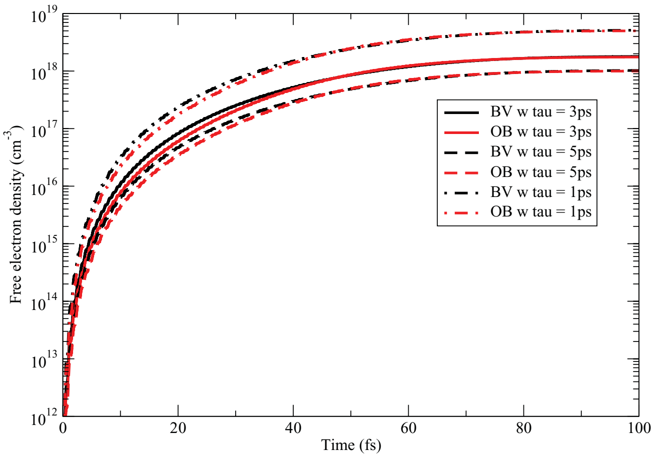

FIG. 2. (Color online) Evolution of the free electron density as a function of time. The relaxation constant is set to 1, 3, and 5 ps. The values of the parameters are the same as described in the caption to Fig. 1.

We now have to check the ability of the present approaches to account for the simultaneous absorption of several photons. To do so, one can study the evolution of the electronic density as a function of the photon energy. Figure 3(a) shows this evolution as predicted by the BVkP approach in the cases where only one conduction state is present and with 40 conduction states (in this case, the energy difference between two adjacent states has been set to $\Delta E = 0.045$ eV). In the first case, the spectrum consists of narrow peaks (resonance) corresponding roughly to the relation of energy conservation $n\hbar\omega = E_g$, where n is the number of absorbed photons to bridge the band gap. The figure shows that the BVkP model is able to capture a process where up to five photons are involved. For more photons, the associated probability is lower than the tail of the one-photon absorption process (because of the finite duration of the laser pulse, the resonance shape is large, whereas it corresponds to a Dirac δ function for an infinite pulse). In the case where the conduction band is filled with 40 states, more transitions are allowed, leading to a broadening of the peaks.

Figure 3(b) shows the same study as the previous one but carried out with the OB model. When there are only two levels (one for the VB and another one for the CB), there is no peak for an even number of absorbed photons. As described in a previous section, the introduction of an additional valence state renders it possible to account for the absorption of an odd number of photons. This fact is demonstrated by the numerical results when three levels are taken into account. In the case where the CB is filled with 40 levels, a broadening of the resonances can also be observed. In order to compare both models, the results of Figs. 3(a) and 3(b) have been reported in Fig. 3(c) for the case of 40 levels. It appears that the results of both models exhibit the same behavior, with, in particular, a comparable evolution of the ionization rate with respect to the number of involved photons. Note that in the cases of four- and five-photon absorption, the models predict opposite behaviors when the photon energy slightly varies. This fact remains unexplained.

The evolution of the free electron density as a function of the photon energy is displayed in Fig. 4, where the same modeling configurations as those of the previous figure have been used. Since free electrons are nothing but relaxed ionized electrons, the spectra under consideration exhibit the same features as those of Fig. 3: Absorption of several photons is well captured by these models. Further, this figure exhibits more clearly that the OB model with only two levels cannot account for the two-photon absorption. Note that the curves are smoother than in the previous graph. More precisely, the cardinal sinelike oscillations due to the finite duration of the pulse disappear [33]. This behavior is due to the fact that various conduction states (with various energies) contribute to the filling of the

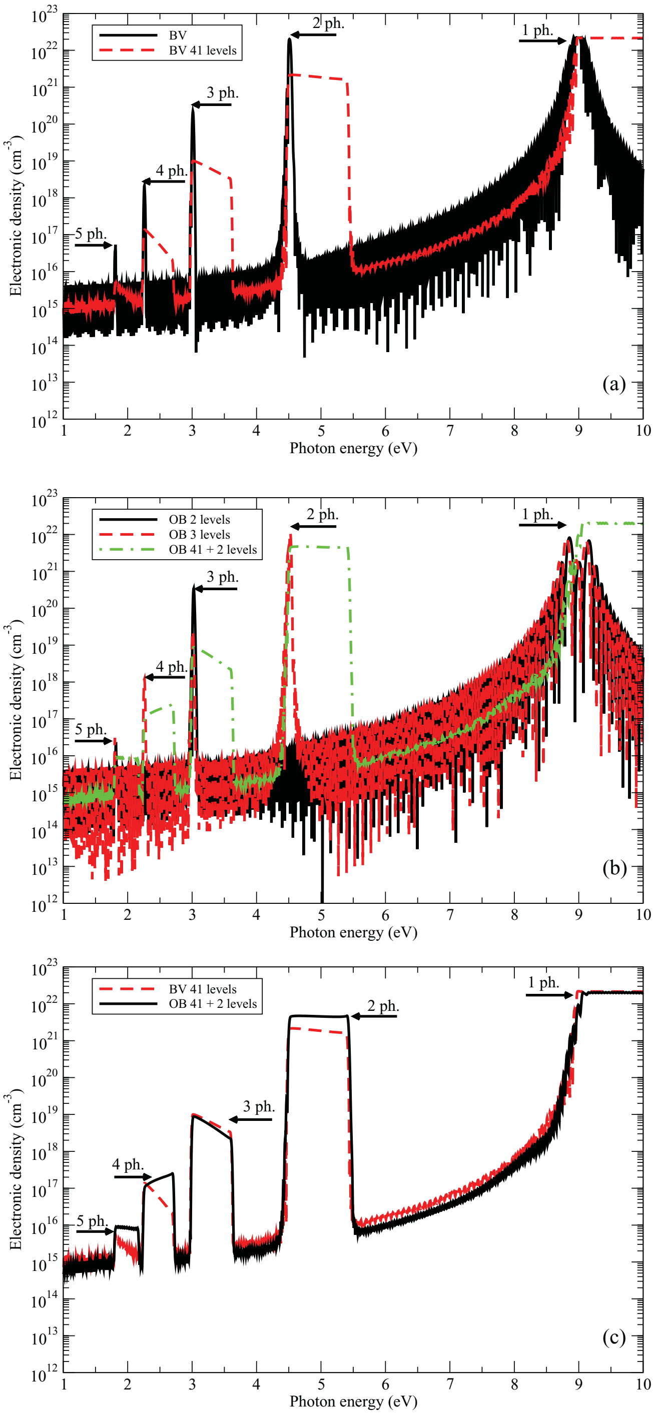

FIG. 3. (Color online) Evolution of the electronic density in the conduction band as a function of the photon energy at $t = \tau$. The curves correspond to predictions of (a) the BVkP model with 2 energy levels and 41 energy levels and of (b) the MB model with 2 energy levels, 3 energy levels, and 41 energy levels. (c) Comparison between both models with 41 levels in the CB. The laser pulse parameters are as follows: $I_0 = 5 \times 10^{13}$ W/cm^2 and $\tau = 100$ fs.

free electronic state. Since there is no coherence between the various contributions, destructive interferences occur and so the total evolution is smooth. Also note that the absorption corresponding to the largest multiphoton order do not appear so clearly as in the previous graph: Resonance can be observed only up to three photons. Absorption up to five photons is obviously taken into account as for the transition from the VB to the CB, but orders larger than 4 are hidden by lower orders, the first in particular, whose tail can be observed down to 3 eV. Actually, in the case of relaxed electrons, significant contributions may come from early ionization, for which the laser intensity has not reached its maximum value, resulting in lower probabilities for high-order multiphoton processes compared to the one-photon absorption, which is less sensible to intensity variations, i.e., the ratio of highly nonlinear to linear dependence with respect to the intensity.

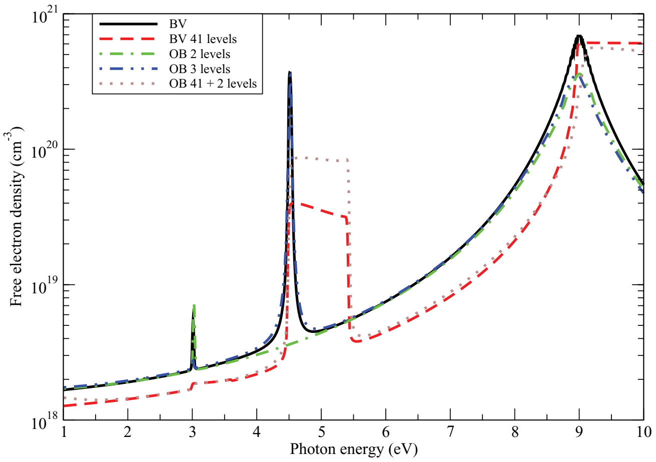

FIG. 4. (Color online) Evolution of the free electron density as a function of the photon energy at $t = \tau$. The values of the parameters are the same as described in the caption to Fig. 3.

In order to further support the fact that our models are able to capture the physics of multiphoton absorption, and to shed light on the behavior with respect to the laser intensity, the evolution of the electronic density at $t = \tau$ is plotted as a function of this laser parameter in Fig. 5. The same modeling configurations as those of the previous figures are used and the calculations have been performed with $\tau = 100$ fs and $\lambda = 413$ nm. In the perturbative regime where the rate of ionization by n photons is proportional to the laser intensity at the n-th power, the slope of the electron density as a function of the laser intensity plotted within a log-log scale is expected to be $n = 3$ in the present case. From Fig. 5, the perturbative region corresponding to the absorption of three photons corresponds roughly to the range [2×10^{11} W/cm^2; 5×10^{12} W/cm^2]. For intensities lower than 2×10^{11} W/cm^2, the smaller slope indicates that the ionization is dominated by the tail of the one-photon absorption. A larger intensity is required to excite the nonlinear three-photon absorption process. Roughly above 5×10^{12} W/cm^2, the electronic density no longer increases, indicating that the nonperturbative regime stands where the ionization probability does not depend much on the multiphoton order [34]. Except in the OB with only two levels, the various models provide a slope that is between 2.88 and 3.07, which is consistent with the expected value $n = 3$. The OB with two levels provides a slope of 2.52, slightly lower than the expected value, revealing again the flaw of this approach to describe accurately all multiphoton orders.

The convergence of our approaches with respect to the number of levels in the CB and to the time step has been checked.

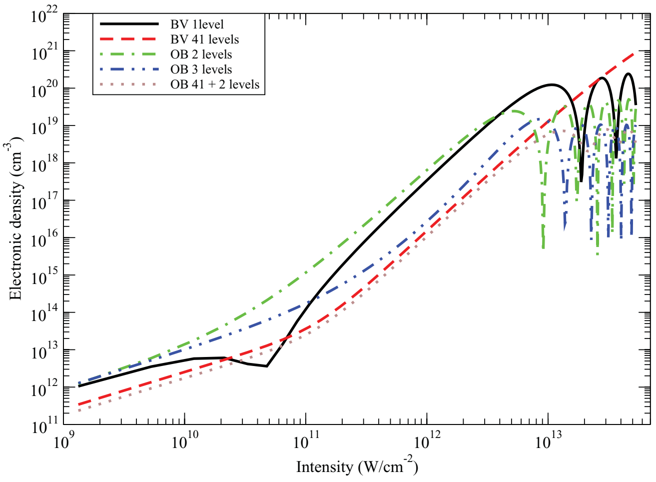

FIG. 5. (Color online) Evolution of the electronic density in the conduction band as a function of the laser intensity at $t = \tau$. The various curves correspond to predictions of the BVkP model with 2 energy levels and 41 energy levels and of the MB model with 2 energy levels, 3 energy levels, and 41 energy levels. The laser pulse parameters are as follows: $\lambda = 413$ nm and $\tau = 100$ fs. Due to the log-log scale, the slope of the straight line directly provides the multiphoton order (which must be equal to 3 with a reliable model).

The results are displayed in Fig. 6, where combinations of 11 levels, 41 levels, and 20 000 and 50 000 time steps have been used. Calculations show that the numerical convergence for the time integration is reached when at least 20 000 time steps are used for a 100-fs laser pulse. When the energy difference between two adjacent states is lower than the energy bandwidth of the laser pulse (in the case of 41 levels), whatever the photon energy (but always leading to the same number of absorbed photons), a transition from the VB to the CB is allowed. This leads to a plateau whose width accounts for the CB structure. If the CB is not discretized enough (11 levels), despite the natural pulse bandwidth, a transition between two adjacent states may be forbidden. This leads to a noisylike spectrum instead of a plateau, as shown by Fig. 6.

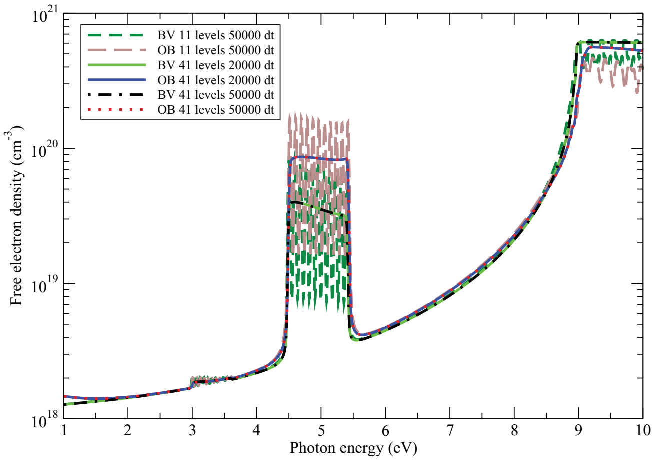

FIG. 6. (Color online) Evolution of the free electron density in the conduction band as a function of the photon energy at $t = \tau$ for both models. The various curves show the convergence of the numerical results with respect to the number of energy levels and the number of time steps.

B. Application to the case where a second harmonic pulse is present

The models under consideration have been developed within the goal of describing the multiphoton absorption during the course of propagation of a laser pulse through an active optical component, i.e., whatever the instantaneous frequency spectrum of the laser pulse. Under these conditions, multiphoton absorption can be induced by various frequencies. For instance, in the case of propagation through a frequency converter crystal, an ionization path may involve absorption of photons of energy $\hbar\omega$ and $2\hbar\omega$, whatever the value of the fundamental frequency ω.

The influence of superposing a second, shorter, wavelength is presented in Fig. 7, which shows the evolution of the free electron density as a function of time. Indeed, as predicted by both approaches, the evolution of the free electron density is significantly enhanced just by adding a second harmonic pulse whose intensity is only 4% of the fundamental wavelength. Note that both models provide almost the same variations.

In order to check the ability of the present approaches to account for possible complex ionization paths, the evolution of the free electron density with respect to the fundamental photon energy (1ω) is plotted in Fig. 8. As for Fig. 7, a second harmonic (2ω) of the fundamental frequency is superimposed with an intensity of 4% of the fundamental. In the case where one photon at 1ω is sufficient to bridge the band gap, the 2ω pulse does not modify the free electron density significantly. Indeed, the 2ω pulse cannot change the photoionization order with a fundamental photon energy larger than the band gap. Its contribution is to promote valence electrons to highly excited conduction states directly. In the case where two photons at 1ω are required (4.5 eV), only one photon at 2ω allows bridging of the band gap, resulting in a significant enhancement of the free

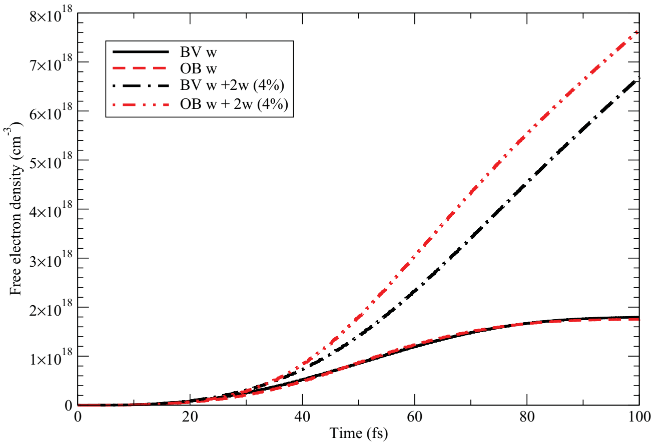

FIG. 7. (Color online) Evolution of the free electron density as a function of time. The legend and the values of the parameters are the same as in Fig. 2. The difference is that a second harmonic laser pulse is superposed to the fundamental pulse in order to simulate conditions that may occur in the course of laser propagation. The characteristics of this additional laser pulse are as follows: $I_2 = 0.04 I_1$, $\tau = 100$ fs, and $\lambda_2 = \lambda_1/2 = 206.5$ nm.

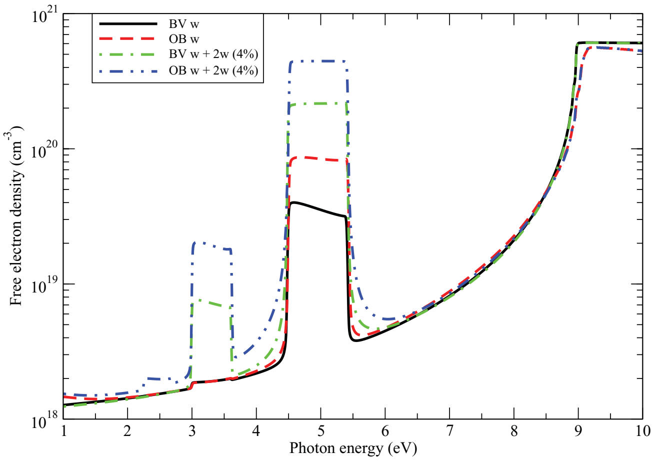

FIG. 8. (Color online) Evolution of the free electron density as a function of the photon energy at $t = \tau$. As in Fig. 7, the results correspond to the case where a 2ω pulse is present. The values of the parameters are the same as described in the caption to Fig. 7.

electron density despite the low 2ω intensity. For this photon energy, 1ω and 2ω pulses lead to two independent ionization paths at the edge, corresponding to the plateau region around 5 eV. However, it can be observed that when the photon energy decreases below 4.5 eV, the free electron density predicted with $1\omega + 2\omega$ does not decrease as sharply as the 1ω case. This is the signature of complex ionization paths where both the fundamental photon energy and its second harmonic contribute together to the ionization: One-photon absorption at 2ω is not enough to bridge the gap, but the simultaneous absorption of a 2ω photon and a 1ω photon allows the transition. The influence of the second harmonic appears more significantly for a fundamental photon energy of 3 eV. In that case, instead of three photons at 1ω, only two photons at 2ω are required, leading to a an increase in the free electron density of one order of magnitude, again despite the low intensity of the second harmonic.

This prediction indicates that, during its course of propagation in a frequency converter crystal, an intense laser pulse may significantly be absorbed due to the enhancement of the ionization rate (when the number of photons required to bridge the band gap is decreasing) and the subsequent heating of the conduction electrons (essentially by the fundamental pulse according to the Drude model, which indicates that the lower the laser frequency, the more efficient the heating).

C. Application to the case of a chirped pulse

Another physical case of interest is the one of a chirped pulse (CP) with a frequency depending on time. This physical situation corresponds exactly to the one for which the present approaches have been designed. As an example, we consider a super-Gaussian pulse of the order 20 of a duration of 534 fs (at $1/e$, from 133 to 667 fs) and a peak intensity of 8×10^{13} W/cm^2. The wavelength varies from 300 to 600 nm

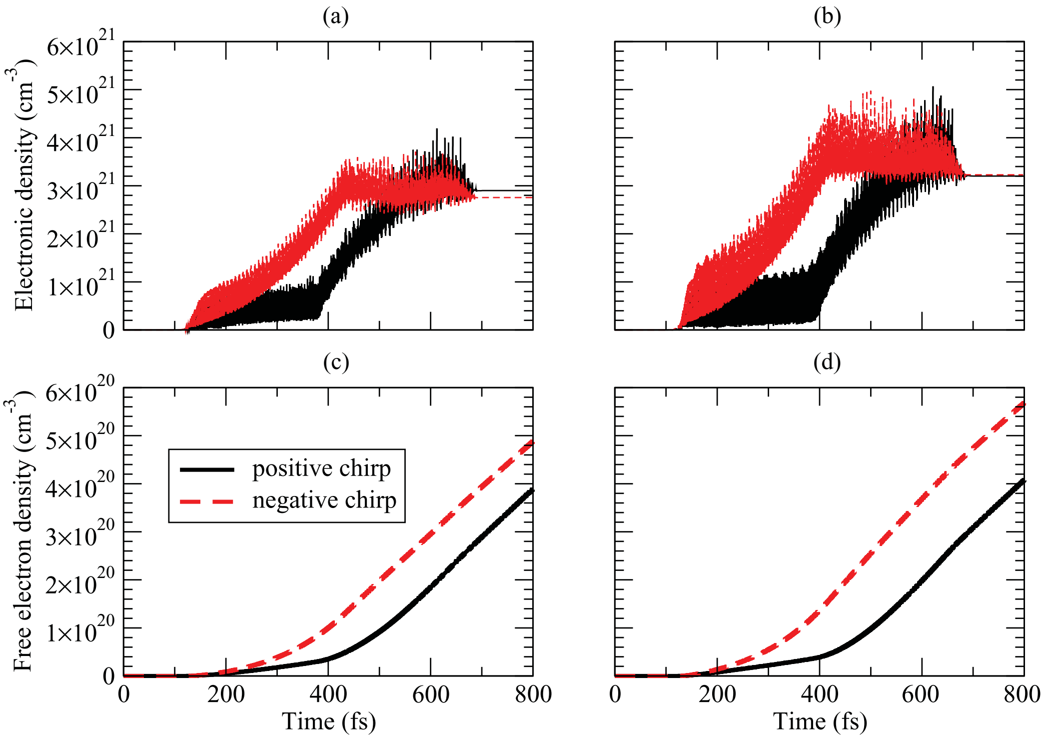

FIG. 9. (Color online) Evolution of [(a) and (b)] the electronic density and of [(c) and (d)] the free electronic density as a function of time for chirped pulses. The left [(a) and (c)] and right [(b) and (d)] graphs correspond to the BVkP and OB predictions, respectively. For these calculations, a super-Gaussian pulse of order 20 and of duration 534 fs (at $1/e$, from 133 to 667 fs) and a peak intensity of 8×10^{13} W/cm^2 was used. The wavelength varies from 300 to 600 nm within the pulse. A linear evolution of the photon energy as a function of time has been chosen: An increase in photon energy corresponds to the black curves (positive chirp), whereas a decrease in the photon energy corresponds to the red curves (negative chirp).

within the pulse. A linear evolution of the photon energy as a function of time within this wavelength interval has been chosen. Two cases are considered: For the first pulse, CP1, the wavelength increases (negatvie chirp), whereas it decreases for the second pulse CP2 (positive chirp).

Predictions of the BVkP and OB approaches under such conditions are reported in Fig. 9. The calculations have been performed by using 100 levels in the CB. For both models, the evolution of the electronic density and of the free electronic density as a function of time are provided in top and bottom graphs, respectively. The left and right graphs correspond to the BVkP and OB predictions, respectively. Let us, first, analyze the BVkP predictions. Considering Fig. 9(a), whatever the chirp, it appears that the curve mainly consists of two parts. Regarding CP1-induced ionization, it increases steadily up to roughly 425 fs, where it no longer evolves. Regarding CP2-induced ionization [the black curve of Fig. 9(a)], it also increases steadily during roughly the first half of the pulse; however, with an average slope smaller than the one of the CP1 case. At $t \simeq 375$ fs, the average slope suddenly increases to a value close to the one of the CP1 case in the first part of the pulse. These sudden variations suggest that the multiphoton order changes during the course of the interaction. Indeed, we have checked that the number of photons varies from 3 to 4 with a CP1 (or from 4 to 3 with CP2) around 400 fs. In Fig. 9(a), the OB model provides very similar trends. It thus appears that the present approaches are well designed to catch the influence of a time-dependent laser frequency on the ionization process. The evolution of the free electronic density, as predicted by both models [Figs. 9(c) and 9(d)], reflects the previously discuted behavior: It consists of two parts with steadily increasing density but with different slopes, accounting for different numbers of absorbed photons depending on time. We have performed other calculations (not presented here) with different laser parameters that allow one to vary the number of absorbed photons by two units. The evolution of the electronic density with respect to time then mainly consists of three parts with sudden changes in the slope, corresponding to a change in the number of absorbed photons. These calculations thus confirm the proposed interpretation of results of Fig. 9.

IV. CONCLUSION AND OUTLOOKS

In order to account for the possible frequency spectrum evolution of the laser pulse during its course of propagation, an ionization model with an arbitrary shape of the laser electric field is necessary. A powerful method that satisfyies this condition is *ab initio* numerical resolution of the time-dependent Schrödinger equation (TDSE). However, with the current computer facilities, it is unrealistic to couple it to a code solving the 3D Maxwell's equations numerically. We thus proposed two simpler approaches, both relying on the dipole approximation and considering a single-active electron within the length gauge. One method is based on the Volkov states that allow us to describe the electron dynamics in both the laser electric and crystalline potentials. The second approach solves the TDSE within the density matrix framework, with specific developments accounting for multiphoton absorption and allowing efficient numerical calculations. Whereas the first model is easy to implement and allows fast calculations, the second approach offers a ladder for further improvements, such as a simple description of the free electron heating by adding coupling between conduction states.

In order to check the reliability of both models and compare their predictions, the dependence of the ionization rate on the laser intensity and frequency was studied, confirming that multiphoton absorption is correctly described. Further, from a general point of view, both approaches provide equivalent predictions. In the case where the laser pulse contains the fundamental frequency and the second harmonic, as in the case of frequency conversion, even a relatively low intensity of a second harmonic may lead to a significant increase in the ionization rate. For pulse propagation through a frequency converter crystal, a code solving the full 3D Maxwell's equations is, therefore, expected to lead to dramatic consequences on the energy deposition in the material. Finally, for chirped pulses, the present models have been shown to correctly account for possible changes in the multiphoton order during the course of interaction. This influence may lead to significant variations of the density of conduction electrons, and consequences on laser-induced material modifications are expected.

ACKNOWLEDGMENTS

Vladimir Tikhonchuk and Henri Bachau are gratefully acknowledged for helpful discussions and comments regarding the present manuscript. Ludovic Hallo is acknowledged for supporting this work.

APPENDIX A: CONSIDERATIONS REGARDING THE BVkP APPROACH

Let us introduce a dipole matrix element in a one-dimensional space X_1. It reads,

$$X_1 = \int_0^\infty dx \phi_c x \phi_v. \tag{A1}$$

In order to evaluate the matrix element of the position operator to the power n, we assume that the wave function for conduction electrons can be approximated by a plane wave as $\phi_c \propto \exp(ikx)$. In that case, one has

$$X_n = \int_0^\infty dx \phi_c x^n \phi_v = \left(-i\frac{\partial}{\partial k}\right)^{n-1} X_1. \tag{A2}$$

If we now assume that a valence electron can be well described by a hydrogenic state, i.e., $\phi_v \propto \exp(-\alpha x)$, then we can show the following relation:

$$X_n = \frac{(-1)^{n-1} n!}{(-\alpha + ik)^{n-1}} X_1. \tag{A3}$$

Under the previous assumptions, it follows that

$$M_n(t) = \frac{[iA(t)]^n (-1)^n (n+1)!}{(-\alpha + ik)^n} M_0(t). \tag{A4}$$

Note that the previous considerations assume at least the following:

(a) The cristalline periodic potential is sufficiently weak to model a conduction electron by a plane wave, i.e., the periodic part of the Bloch wave function, usually called $u_{\vec{k}}(\vec{r})$, is a constant close to unity.

(b) The electronic density in the conduction band is assumed to be not too high, allowing one to model a conduction electron by a free plane wave, i.e., without the influence of electron-electron collisions.

(c) The valence hydrogenic state is derived from a Coulomb potential. This assumption is valid as long as the electronic density is not too high. For a relatively high density, a screened Coulomb potential should be used, leading to a different expression for the valence state.

(d) In the case of dielectric materials with generally more complex atoms than hydrogen, a potential that differs from a pure Coulomb one should be used, also leading to a different expression of the valence wave function. However, this improvement is not expected to modify the predicted trends of the present paper.

(e) A tight binding approach, accounting for periodic conditions, may provide a better evaluation of the previous integral; however, the scaling with n should not be significantly changed.

APPENDIX B: CONSIDERATIONS REGARDING THE OPTICAL BLOCH APPROACH

With the BVkP approach we can get multiphoton ionization at any order even with only two levels. This is no longer true for the optical Bloch approach. In this Appendix, we give some explanations for this fact.

If we set $\mathbf{E}(t) = E_0\mathbf{e}(t)$, assuming the form of Eq. (20) and the choice of the matrix μ [38], the element of the density matrix can be expanded in powers of E_0 as

$$\rho_{11} = \sum_{k=0}^{\infty} E_0^{2k}\rho_{11}^{(2k)}(t), \tag{B1}$$

$$\rho_{22} = 1 - \rho_{11}, \tag{B2}$$

and

$$\rho_{12} = \sum_{k=0}^{\infty} E_0^{2k+1}\big(\widehat{\rho}_{12}^{(2k+1)} + i\,\widetilde{\rho}_{12}^{(2k+1)}\big). \tag{B3}$$

To solve optical Bloch equations is, thus, equivalent to solve successively the equations

$$\frac{1}{\omega_{12}^2}\frac{\partial^2}{\partial t^2}\widehat{\rho}_{12}^{(2k+1)}(t) + \widehat{\rho}_{12}^{(2k+1)}(t) = -2\,[\mathbf{e}(t)\cdot\mu]\,\rho_{11}^{(2k)}(t), \tag{B4}$$

$$\widetilde{\rho}_{12}^{(2k+1)} = \frac{\partial}{\partial t}\rho_{12}^{(2k+1)}(t), \tag{B5}$$

and

$$\frac{\partial}{\partial t}\rho_{11}^{(2k+2)}(t) = 2\,[\mathbf{e}(t)\cdot\mu]\,\widetilde{\rho}_{12}^{(2k+1)} \tag{B6}$$

with

$$\rho_{11}^{(0)} = 1. \tag{B7}$$

Thus, if $\mathbf{e}(t)$ is a periodic function with frequency f, $\widehat{\rho}_{12}^{(2k+1)}$is a sum of periodic functions whose frequencies are odd multiples of f, while $\rho_{11}^{(2k)}$is a sum of periodic functions whose frequencies are even multiples of f. Since in our case ρ_{22} corresponds to the ionization rate, resonances will occur only by integrating equations for $\widehat{\rho}_{12}^{(2k+1)}(t)$ and, thus, for odd multiples of the laser frequency f. This explains why, with the two levels, optical Bloch equations cannot describe multiphoton ionization with an even number of photons.

APPENDIX C: INVERSION OF THE MATRIX $[\mathbf{Id} + \frac{i}{2}\boldsymbol{H}(t + \frac{\delta t}{2})]$ FOR THE OPTICAL BLOCH APPROACH

For the optical Bloch approach we need to invert the matrix $M = [\mathrm{Id} + \frac{i}{2}H(t + \frac{\delta t}{2})]$. We have two levels in the valence band and n levels in the conduction band. Since we have hypothesized that there is no interaction between the conduction band levels, the matrix M can be written as follows:

$$M = \begin{pmatrix} A & B \\ C & D \end{pmatrix}, \tag{C1}$$

where A, B, C, and D are 2×2, $2 \times n$, $n \times 2$, and $n \times n$ matrices, respectively. D is a diagonal matrix with no zero on the diagonal. Moreover, for $\delta t = 0$ the matrix M is the identity matrix and, thus, for small-enough δt, M is invertible and the following formal computations will be valid. For any couple of vectors U and V with respectively two and n components, we have to find two similar vectors X and Y such that

$$\begin{pmatrix} A & B \\ C & D \end{pmatrix}\begin{pmatrix} X \\ Y \end{pmatrix} = \begin{pmatrix} U \\ V \end{pmatrix}.$$

We notice, first, that Y verifies $Y = D^{-1}(V - CX)$. This leads, then, to $(A - BD^{-1}CX)X = U - BD^{-1}V$.

The matrix $T = (A - BD^{-1}CX)$ is an invertible 2×2 matrix. We get, therefore, $X = T^{-1}(U - BD^{-1}V)$ and, finally,

$$M^{-1} = \begin{pmatrix} T^{-1} & -T^{-1}BD^{-1} \\ -D^{-1}CT^{-1} & D^{-1}CT^{-1}BD^{-1} + D^{-1} \end{pmatrix}. \tag{C2}$$

This result is still valid if we add an additional level to account for the irreversibility of photoionization. Therefore, the only nontrivial operation required to invert the matrix M is the inversion of a 2×2 matrix T.

---

[1] B. C. Stuart, M. D. Feit, A. M. Rubenchik, B. W. Shore, and M. D. Perry, Phys. Rev. Lett. **74**, 2248 (1995).

[2] B. Rethfeld, Phys. Rev. B **73**, 035101 (2006).

[3] M. D. Perry, B. C. Stuart, P. S. Banks, M. D. Feit, V. Yanovsky, and A. M. Rubenchik, J. Appl. Phys. **85**, 6803 (1999).

[4] B. N. Chichkov, C. Momma, S. Nolte, F. von Alvensleben, and A. Tnnermann, Appl. Phys. A **63**, 109 (1996).

[5] T. E. Itina, N. Shcheblanov, J.-P. Colombier, R. Stoian, E. Audouard, T. Y. Derrien, R. Torres, J. Hermann, M. E. Povarnitsyn, and K. V. Khishchenko, AIP Conf. Proc. **1278**, 38 (2010).

[6] J. R. Gulley, Proc. SPIE **7842**, 78420U (2010).

[7] J. R. Gulley and W. M. Dennis, Phys. Rev. A **81**, 033818 (2010).

[8] L. Berge, S. Skupin, R. Nuter, J. Kasparian, and J.-P. Wolf, Rep. Prog. Phys. **70**, 1633 (2007).

[9] A. Bourgeade and B. Nkonga, Multiscale Model. Simul. **4**, 1059 (2005).

[10] A. Bourgeade, C. Mezel, and O. Saut, J. Sci. Comput. **44**, 170 (2010).

[11] C. Mezel, A. Bourgeade, and L. Hallo, Phys. Plasmas **17**, 113504 (2010).

[12] L. V. Keldysh, Sov. Phys. JETP **6**, 763 (1958).

[13] L. V. Keldysh, Sov. Phys. JETP **20**, 1307 (1965).

[14] A. M. Perelomov, V. S. Popov, and M. V. Terent'ev, Sov. Phys. JETP **23**, 924 (1966).

[15] A. M. Perelomov and V. S. Popov, Sov. Phys. JETP **25**, 336 (1967).

[16] M. V. Ammosov, N. B. Delone, and V. P. Krainov, Sov. Phys. JETP **64**, 1191 (1986).

[17] P. Bala, J. Matulewski, A. Raczynski, and J. Zaremba, Phys. Rev. A **57**, 4561 (1998).

[18] K. Babiarz, A. Raczynski, and J. Zaremba, Phys. Rev. A **64**, 045401 (2001).

[19] V. S. Popov, Phys. Usp. **47**, 855 (2004).

[20] W. V. Houston, Phys. Rev. **57**, 184 (1940).

[21] J. Callaway, *Quantum Theory of the Solid State* (Academic Press, New York, 1974).

[22] L. M. Narducci, S. S. Mitra, R. A. Shatas, P. A. Pfeiffer, and A. Vaidyanathan, Phys. Rev. B **14**, 2508 (1976).

[23] J. von Neumann, *Mathematische Grundlagen der Quantenmechanik* (Springer-Verlag, Berlin, 1932).

[24] C. Cohen-Tannoudji, J. Dupont-Roc, and G. Grynberg, *Atom-Photon Interactions: Basic Process and Applications* (Wiley-VCH Verlag, New York, 2004).

[25] B. Cagnac and J. P. Faroux, *Lasers* (EDP Sciences, Les Ulis, 2002).

[26] H. R. Reiss and V. P. Krainov, Phys. Rev. A **50**, R910 (1994).

[27] M. Jain and N. Tzoar, Phys. Rev. A **18**, 538 (1978).

[28] G. Duchateau, E. Cormier, H. Bachau, and R. Gayet, Phys. Rev. A **63**, 053411 (2001).

[29] G. Duchateau, E. Cormier, and R. Gayet, Phys. Rev. A **66**, 023412 (2002).

[30] R. Gayet, J. Phys. B **38**, 3905 (2005).

[31] D. G. Arbo, J. E. Miraglia, M. S. Gravielle, K. Schiessl, E. Persson, and J. Burgdörfer, Phys. Rev. A **77**, 013401 (2008).

[32] A. Maquet, B. Piraux, A. Scrinzi, and R. Taïeb, Phys. Rev. A **74**, 027401 (2006).

[33] C. Cohen-Tannoudji, B. Diu, and F. Laloé, *Quantum Mechanics* (Wiley-VCH Verlag, Berlin, 2006).

[34] H. D. Jones and H. R. Reiss, Phys. Rev. B **16**, 2466 (1977).

[35] N. W. Ashcroft and N. D. Mermin, *Solid State Physics* (Holt, Rinehart and Winston, New York, 1976).

[36] B. Bidégaray, A. Bourgeade, D. Reignier, and R. W. Ziolkowski, *Multi-level Maxwell-Bloch Simulations, in Mathematical and Numerical Aspects of Wave Propagation*, edited by A. Bermúdez, D. Gómez, C. Hazard, P. Joly, and J. E. Roberts (SIAM, Philadelphia, INRIA, Rocquencourt, FR, 2000), pp. 221–225.

[37] C. Besse, B. Bidegaray-Fesquet, A. Bourgeade, P. Degond, and O. Saut, M2AN **38**, 321 (2004).

[38] R. Loudon, *The Quantum Theory of Light* (Clarendon Press, Oxford, 1973).

[39] G. Duchateau, G. Geoffroy, A. Dyan, H. Piombini, and S. Guizard, Phys. Rev. B **83**, 075114 (2011).

[40] P. Martin, S. Guizard, Ph. Daguzan, G. Petite, P. D'Oliveira, P. Meynadier, and M. Perdrix, Phys. Rev. B **55**, 5799 (1997).

[41] S. Guizard, P. D'Oliveira, Ph. Daguzan, Ph. Martin, P. Meynadier, and G. Petite, Nucl. Instrum. Methods B **116**, 43 (1996).

[42] F. Quere, S. Guizard, and Ph. Martin, Europhys. Lett. **56**, 138 (2001).

[43] T. Otobe, J. Phys.: Condens. Matter **22**, 384204 (2010).

[44] T. Otobe, M. Yamagiwa, J.-I. Iwata, K. Yabana, T. Nakatsukasa, and G. F. Bertsch, Phys. Rev. B **77**, 165104 (2008).